Journal of the Korean Chemical Society
2012, *Vol. 56, No. 4*
Printed in the Republic of Korea
http://dx.doi.org/10.5012/jkcs.2012.56.4.448

The Electrochemical Behavior of Ni-base Metallic Glasses Containing Cr in H_2SO_4 Solutions

Sanaa. T. Arab†, Khadijah. M. Emran* and Hamad A. Al-Turaif‡

*Applied Chemistry Department, College of Applied Science, Taibaj University, Al-Madinah Al-Monawarah, Kingdom of Saudi Arabia. *E-mail: kabdalsamad@taibahu.edu.sa*

†Department of Chemistry, Girls' College of Education, King Abdulaziz University, P.O(2321), Jeddah 21451, Kingdom Saudi Arabia

‡Department of Chemical and Materials Engineering, King Abdulaziz University Jeddah, Kingdom Saudi Arabia

(Received December 5, 2008; Accepted May 6, 2009)

ABSTRACT. In order to develop alloy resistance in aggressive sulphat ion, the corrosion behavior of metallic glasses $Ni_{92.3}Si_{4.5}B_{32,}$ $Ni_{82,3}Cr_7Fe_3Si_{4.5}B_{3.2}$ and $Ni_{75.5}Cr_{13}Fe_{4.2}Si_{4.5}B_{2.8}$ (at %) at different concentrations of H_2SO_4 solutions was examined by electrochemical methods and Scanning Electron Microscope (SEM) and X-ray Photoelectron Microscopy (XPS) analyses. The corrosion kinetics and passivation behavior was studied. A direct proportion was observed between the corrosion rate and acid concentration in the case of $Ni_{92.3}Si_{4.5}B_{32}$ and $Ni_{75.5}Cr_{13}Fe_{4.2}Si_{4.5}B_{2.8}$ alloys. Critical concentration was observed in the case of $Ni_{82,3}Cr_7Fe_3Si_{4.5}B_{3.2}$ alloy. The influence of the alloying element is reflected in the increasing resistance of the protective film. XPS analysis confirms that the protection film on the $Ni_{92.3}Si_{4.5}B_{32}$ alloy was NiS which is less protective than that formed on Cr containing alloys. The corrosion rate of $Ni_{82,3}Cr_7Fe_3Si_{4.5}B_{3.2}$ and $Ni_{75.5}Cr_{13}Fe_{4.2}Si_{4.5}B_{2.8.}$ alloys containing 7% and 13% Cr are 7.90-26.1×10^{-3} mm/y which is lower about 43-54 times of the alloy $Ni_{92.3}Si_{4.5}B_{32}$ (free of Cr). The high resistance of $Ni_{75.5}Cr_{13}Fe_{4.2}Si_{4.5}B_{2.8}$ alloy at the very aggressive media may due to thicker passive film of Cr_2O_3 which hydrated to hydrated chromium oxyhydroxide.

Key words: Nickel base alloys, Metallic glasses, Passivity, Role of chromium, Corrosion

INTRODUCTION

The structure of alloying materials is often found in the form of amorphous, crystalline or metastable. Amorphous alloys are metals and metal alloys with no long range atomic order; also known as glassy alloys, metallic glasses, or non-crystalline alloys.

Formation of alloys have long been used to form new materials with specific properties depending on the alloying elements, such as how nickel can be used for corrosion resistance, cobalt for magnetic memories, and chromium for decorative purposes. The structure of these alloys can be tailored by controlling the process parameters, such as current density, pH, temperature, and bath composition. It was found that the alloy composition induces the structural and corrosion behavior of amorphous alloys.[1-10]

Due to the lack of long range order and their degree of atomic disorder, amorphous alloys exhibit unique physical, chemical, and mechanical properties, all of which make them superior to their crystalline counterparts. The non-metal atoms, such as B, Si, C, and P are often used as amorphizing agents[11,12] and are usually employed to reduce metals, such as Fe, Co, Ni, Cu, Pb, and Re in the aqueous solution to form composite coatings.

The amorphizing agents usually have dimension less than the metals they bond with.[1,2,4,7]

Several studies reveled the corrosion resistance of Ni–metalloid amorphous alloys and the passivation ability of them in different media.[1,4,5,6,9,10-22]

The present work aims to investigate the beneficial effect of Cr presence on the electrochemical and passivation properties of bulk Ni-base glassy alloy in H_2SO_4 solutions.

EXPERIMENTAL

Specimens and Test Solutions

Ingot $Ni_{92.3}Si_{4.5}B_{32,}$ $Ni_{82,3}Cr_7Fe_3Si_{4.5}B_{3.2}$ and $Ni_{75.5}Cr_{13}Fe_{4.2}Si_{4.5}B_{2.8}$ (at %) alloys were supplied by Vacuumschmelze with physical properties summarized in *Table* 1. Rounded specimens were cut from a foil (2.5-7.5 mm width and 20-50 μm thickness) with a working area of (2.4 mm^2).

Each experiment was carried out with a new strip. The electrodes were decreased with alcohol and rinsed several times with double distilled water and finally cleaned in an ultrasonic bath (Model LF2003, 50160Hz, Dal Trozzo,

***Table* 1.** Some physical properties of studied alloys

Specimens	Electrode	Melting temperature °C	Density gm/cm^3
I	$Ni_{92.3}Si_{4.5}B_{3.2}$	1054	8.07
II	$Ni_{82.3}Cr_7Fe_3Si_{4.5}B_{3.2}$	1024	7.88
III	$Ni_{75.5}Cr_{13}Fe_{4.2}Si_{4.5}B_{2.8}$	1103	7.82

Italy). The electrodes were connected to copper specimen holder and immersed in the test solution with out drying.

As corrosion medium, aerated solutions of H_2SO_4 (Panreac) were used. Appropriate concentrations of the acid were prepared by dilution using be-distilled water.

Methods

Electrochemical measurements have been achieved by connecting the electrochemical cell to ACM Gill AC instrument and to a Samsung computer (Bridge DVD ASUS 8X max). In the conventional cell three – electrode assembly, containing naturally aerated H_2SO_4 solutions, the working electrode was nickel-base glassy alloy (2.4 mm^2), *Table* 1, with platinum wire and saturated calomel electrodes were used for counter and reference electrodes, respectively. Experiments were carried out in stagnant solutions at 30 ºC ±0.1 temperature.

After immersion of the specimen, prior to the impedance measurement, a stabilization period of 15 min was found, which proved sufficient for E_{ss} (the steady-state potential). The AC frequency range extended from 30 kHz to 0.1 Hz, a 10 mV peak to peak sine wave being the excitation signal. The impedance spectra were fitted using a non-linear least – squares fitting procedure developed by Boukamp.[23]

Potentiodynamic polarization curves were obtained with a potential sweep rate of 1 mV/s. The potential was sweep from cathodic to anodic directions after impedance run. Corrosion current densities (I_{corr}) were calculated by extrapolating the Tafel lines to corrosion potential (E_{corr}). Passivation parameters: critical passivation current density (I_{cc}), critical passivation potential (E_{cc}), passivation potential (E_{pass}), passivation current density (I_{pass}) were determined from the potentiodynamic polarization curves.

After the electrochemical test in 3.0 M H_2SO_4, chemical compositions of the alloy surface were measured by XPS using a multi-technique surface analysis system (MAX200, Leybold) with MgKα and AlKα at 100W of x-ray power. The pressure in the analysis chamber during sample analysis was less than 10^{-8} m bar.

The nickel base specimens coated by a film of 50 nm of gold by sputtering, have been investigated by using a XL20–PHILIPS SEM. The data obtained from these experimental methods were compared.

RESULTS AND DISCUSSION

Electrochemical Impedance Spectroscopy (EIS)

The electrochemical impedance spectroscopy (EIS) helps to isolate the individual components describing the particular processes and properties of phases and interfaces, electrolyte resistance, charge transfer resistance (the fast process), double layer capacitance, adsorption and diffusion (the lowest process).[24]

The Nyquist diagrams were characterized by depressed capacitive loops with the theoretical centre located below the real axis. So, the measured capacitive response is not generally ideal (i.e., a pure capacitor). A constant phase element (CPE) is then introduced for the spectra fitting, instead of an ideal capacitance element. The impedance expression of CPE is given by:

$$Z_{CPE} = \frac{1}{Q(j\omega)^n}$$

where Q and n are frequency - independent fit parameters, $j = (-1)^{1/2}$ the imaginary number and $\omega = 2nf$ the angular frequency in radius. The factor n, the CPE exponent, is an adjustable parameters.

For n = 1 the CPE describes an ideal capacitor with Q (mF/cm^2) equal to the capacitance C and the phase angle θ equal to 90^o and for n = 0 the CPE is an ideal resistor and the phase angle equal to 0^o. When n = 0.5 the CPE represents a Warburg impedance with diffusion character and for $0.5 < n < 1$ the CPE describes a frequency dispersion of time constant due to local inhomogeneties in the dielectric material. Inductance characteristics presents when n = -1. In general, it is believed that the CPE is related to some type of heterogeneity of the electrode surface as well as to the fractal nature (roughness or porosity) of the surface.[25,26] Analysis of the impedance spectra was done by fitting the experimental data to equivalent circuit. The quality of fitting to the equivalent circuit (EC) was judged firstly by the Chi- square (χ^2) values and secondly by the error distribution versus frequency, comparing experimental

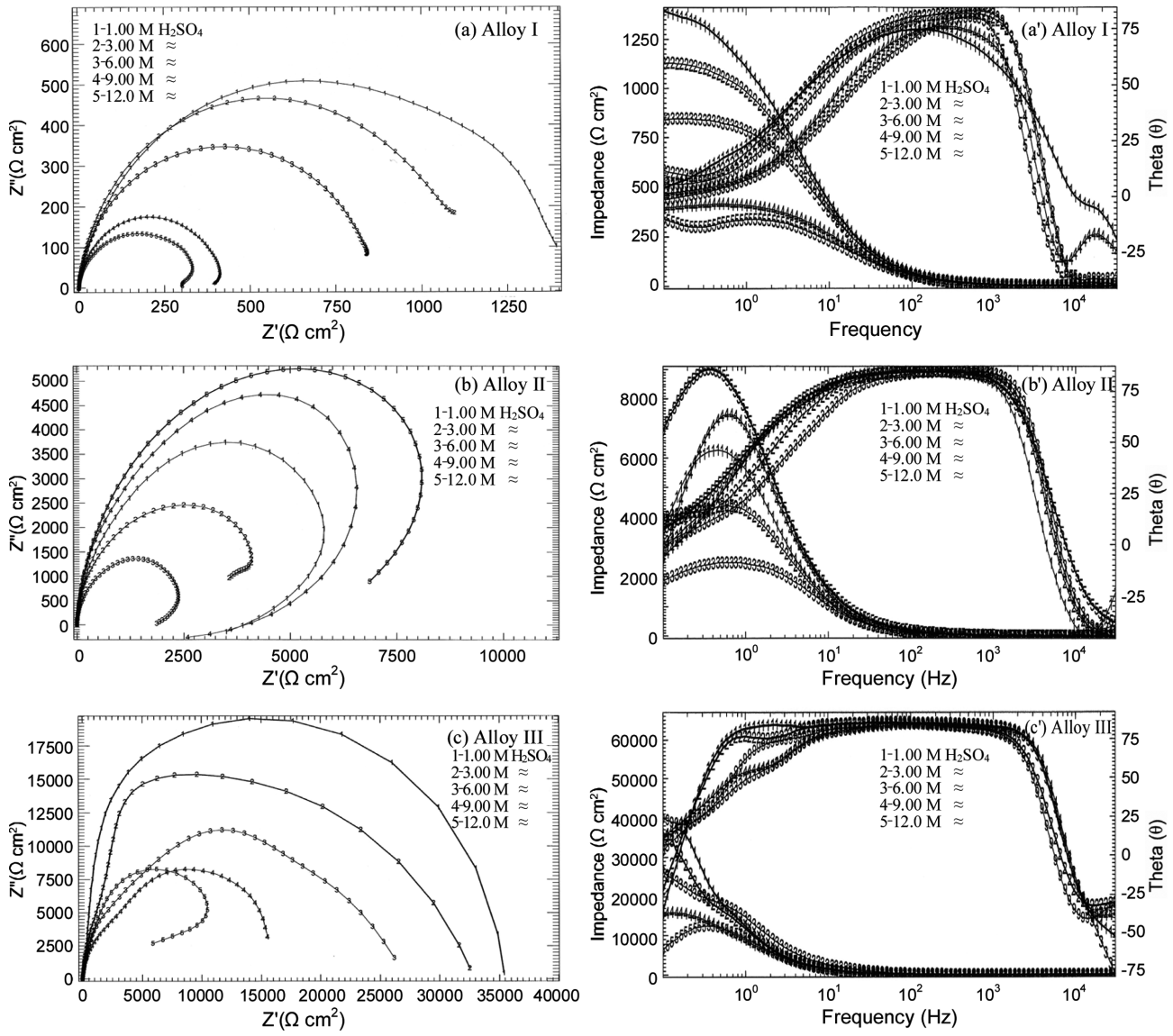

***Fig*. 1.** Impedance plots of Ni-base glasses alloys in different concentrations of H_2SO_4.

with simulated data.

The impedance spectra recorded for alloy I in 1.0, 3.0, 6.0, 9.0 and 12.0 M H_2SO_4 solutions are shown in *Fig.* 1(a) where one capacitive loop is observed irrespective of the sulphat ion concentration with an open end at low frequency at 1.0, 3.0 and 6.0 M H_2SO_4. The corresponding Bode - phase plots are shown in *Fig*. 1(a') where one time constant is obtained, this reveals that there is only one reaction controlling the corrosion process. This reaction is the homogeneous corrosion of the surface in contact with the solution.[27] Only when [H_2SO_4] equals to 12.0 M the impedance plot is a semicircle fallowed by an inductive loop.

The spectra were fitted using (EC) shown in *Fig*. 2(a) (one time - constant circuit) with circuit description code (CDC) R(R_{ct}Q) in the range (1.0-9.0) M and using (EC) shown in *Fig*. 2(b) at 12.0 M with the (CDC) R(Q_1 [R_{ct1}(Q_2R_{ct2})]). Excellent agreement between the fitted and experimental data was obtained ($\chi^2 = 10^{-3}$-10^{-4}).

Table 2 shows the fit parameters for alloy I in different concentrations of H_2SO_4. It is clear from the data that the alloy resistance (R_{ct} values) decreases indicating more dissolution. A sudden decrease occurred at 9.0 M of acid, and the corrosion rate in mm/y goes to opposite direction. The extent of dissolution becomes greater (about 75.7%) as the acid concentration increases to 12.0 M. The size of the

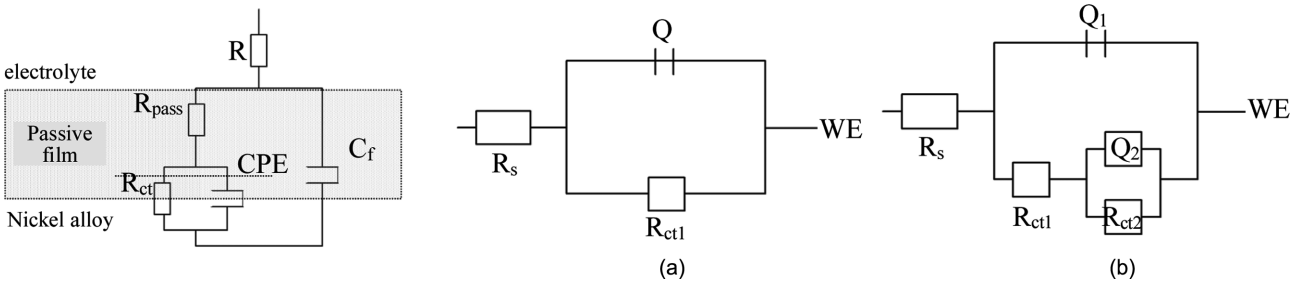

***Fig.* 2.** Electrical equivalent circuit for the interpretation of experimental impedance diagrams of passivated alloy III at 3.0, 6.0 and 9.0 M in H_2SO_4. R_{pass}: electrolytic resistance through the passive film; C_f: film capacity; R_{ct}: charge transfer resistance; CPE: double layer capacity: (a) Equivalent circuit model for the metal suffering general corrosion. R_s: solution resistance; R_{ct1}: charge transfer resistance; Q: double layer capacitance; (b) Equivalent circuit model for the metal suffering localized attack. R_s: solution resistance; R_{ct1}: charge transfer resistance; Q_1: double layer capacitance. R_{ct2}: electrolytic resistance through the pit; Q_2: the pit capacity.

***Table* 2.** Electrochemical kinetic parameters and corrosion rate obtained by EIS technique for Ni-base metallic glasses alloys in naturally aerated H_2SO_4 solutions at 30 °C

Alloy	C_{HCl} (M)	R_{ct} (Ωcm^2)	CPE (Q) ($\mu F/cm^2$)	n	Corrosion rate mm/y
I	01.0	1442	64.89	0.85	0.34
	03.0	1155	63.60	0.87	0.43
	06.0	873.1	64.79	0.86	0.56
	09.0	422.2	65.98	0.88	1.17
	12.0	350.0	88.50	0.82	1.41
II	01.0	6155	17.31	0.83	0.046
	03.0	4516	18.83	0.85	0.063
	06.0	2483	19.66	0.86	0.114
	09.0	7109	13.83	0.85	0.039
	12.0	9820	12.99	0.93	0.029
III	01.0	35950	12.92	0.96	7.90×10^{-3}
	03.0	30630	13.37	0.92	9.27×10^{-3}
	06.0	26270	14.93	0.88	10.8×10^{-3}
	09.0	16420	16.75	0.89	17.3×10^{-3}
	12.0	10870	16.96	0.93	26.1×10^{-3}

semicircle is reduced with an indication of localized attack. The n values listed in *Table* 2 are close to 1 (~ 0.86) at (1.0 to 9.0) M of SO_4^{2-} ion, and it may considered to behave as a capacitor. Values of Q are regularly increase with [H_2SO_4] increase related to more porosity of the protected layer allowing Ni^{+2} to diffuse through it. The Q values were found to be lower than that in HCl solutions.[28]

Nyquist plots and Bode - plots of alloy II in [H_2SO_4] solutions are presented in *Figs*. 1(b,b') respectively. EIS spectra obtained consist of capacitive arc with pseudo inductive loop regardless of the concentration of SO_4^{2-} ions. The phase angle θ_{max} is around 90° suggesting that the electrochemical process occurring at high frequency favors the formation of the passive film.[29] A combination of a capacitive and a pseudo - inductive loop is notecited at the low frequency. Such a combination can be explained to be due to a competitive behavior between acceleration and deceleration (inhibition) process on the alloy surface by the intermediate species.[30]

The results in *Table* 2 indicated that the alloy resistance decreases as the [H_2SO_4] increases up to 6.0 M and then its values increase resulting high values of R_{ct} and low values of corrosion rate (mm/y), but they are still lower in compared with its value in HCl solutions.[28] The increase in the capacity (Q) of the protective layer at 6.0 M HCl indicated the increase in the porosity this layer. The acid diffuses through the layer and reached the alloy at alloy/film interface. Where the low value of Q at high acid concentration reflexes high protective thick film layer of protective film formed on the alloy.

The obtained values of n (~0.86) indicates that the CPE element is associated with low film capacitance and slight low homogeneous of the surface may due to the computation between both the healing and pitting on the oxide

surface.

For impedance spectra of the alloy III in different [H_2SO_4] solution, the semicircle representing the protection film merges with the charge transfer loop. Hence, the EIS spectra for the corrosion test shown in *Figs*. 1(c,c') are described by a simple equivalent circuit as shown in *Fig*. 2.

The lowest frequency capacitive loop seems to change to pseudo inductive loop at 12.0 M H_2SO_4. A pseudo inductive time constant is normally observed for a passive electrode when an increase of the surface fraction causes an increase in the local current at the film / solution interface.

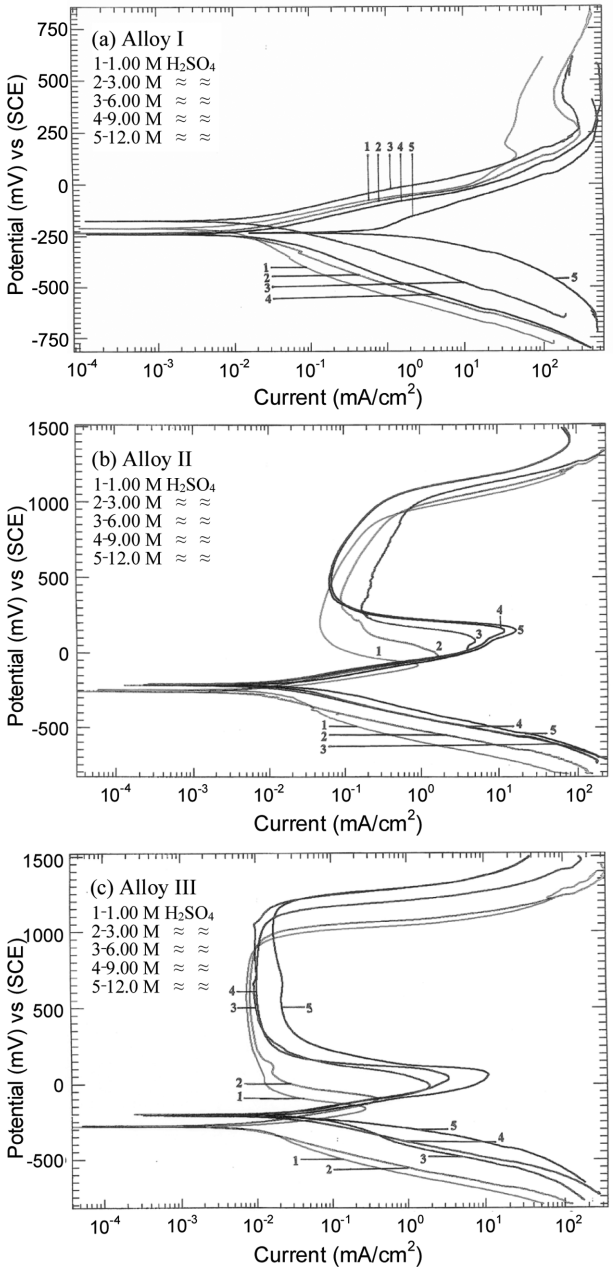

***Fig*. 3.** Potentiodynamic polarization curves of Ni-base metallic glasses alloys different concentrations of H_2SO_4.

As a whole, the tendency to resistance (R_{ct} values) decrease as [H_2SO_4] increases. Corrosion resistance at 12.0 M H_2SO_4 is lower by about 69.76% (3.3 times) than at 1.0 M H_2SO_4. On the other hand, addition of SO_4^{2-} in range (1.0 to 12.0)M results in a regular increase in CPE values indicated the accelerating effect of this ion. These results indicated that the solution reaches the metallic surface by penetrating through the pores or because of the film thickness dissolution causing the decrease of the total system impedance. This hypothesis can be confirmed by time decrease of the capacitive arcs in the Nyquist diagrams and increase the corrosion rate mm/y. The n values listed in *Table* 2 were close to 1(~0.92) and the wider relaxation time constants with maximum phase angle of 85° indicates the capacitor behavior of the alloy III surface which is attributed to a dissolution controlled process.

Potentiodynamic Polarization Study

The potentiodynamic polarization curves of alloy I in H_2SO_4 solutions in the concentration range (1.0-12.0) M H_2SO_4 are shown in *Fig*. 4(a). The cathadic polarization curves are shifted towards increase in hydrogen evolution reaction with increasing acidity of the acid. Also I_{corr} values goes in same direction as shown in *Table* 2.

From curves in *Fig*. 4(a) it can be observed that the alloy exhibit active - passive behavior at 1.0, 3.0 and 6.0 M H_2SO_4 solutions at potentials (E_{cp} = 193, 386 and 442 mV (SCE)) respectively. Values of both the passivation tendency I_{cc}, and degree of passivation I_{Pass}, of the alloy increase appreciably with the increase of acid concentration as shown in *Table* 3. This may indicate that the increase of [H_2SO_4] will accelerate the Ni dissolution in both the active and passive region. Rising of I_{cc} values with the increase of [SO_4^{2-}] indicated that the rate of anodic dissolution on in the active region increases with increasing acidity of the acid, while the increase of I_{pass} values within the passive potential range as the potential shifted in the positive direction can be attributed to the dissolution action of the acid on the passivation film layer and / or the increase in the porosity of protective layer with the increase in the acid concentration.

Pseudo passivation is exhibited by the alloy at 1.0, 3.0 and 6.0 M of H_2SO_4 acid attributed to the stimulation action of low concentration of SO_4^{2-} which adsorbed at the uncovered small anodic area, increasing the cathode / anode area ratio, resulting in a strong shift of potential towards positive E_p values and a concentrate attack on the un passivated regions to create pits and pores resulting in porous

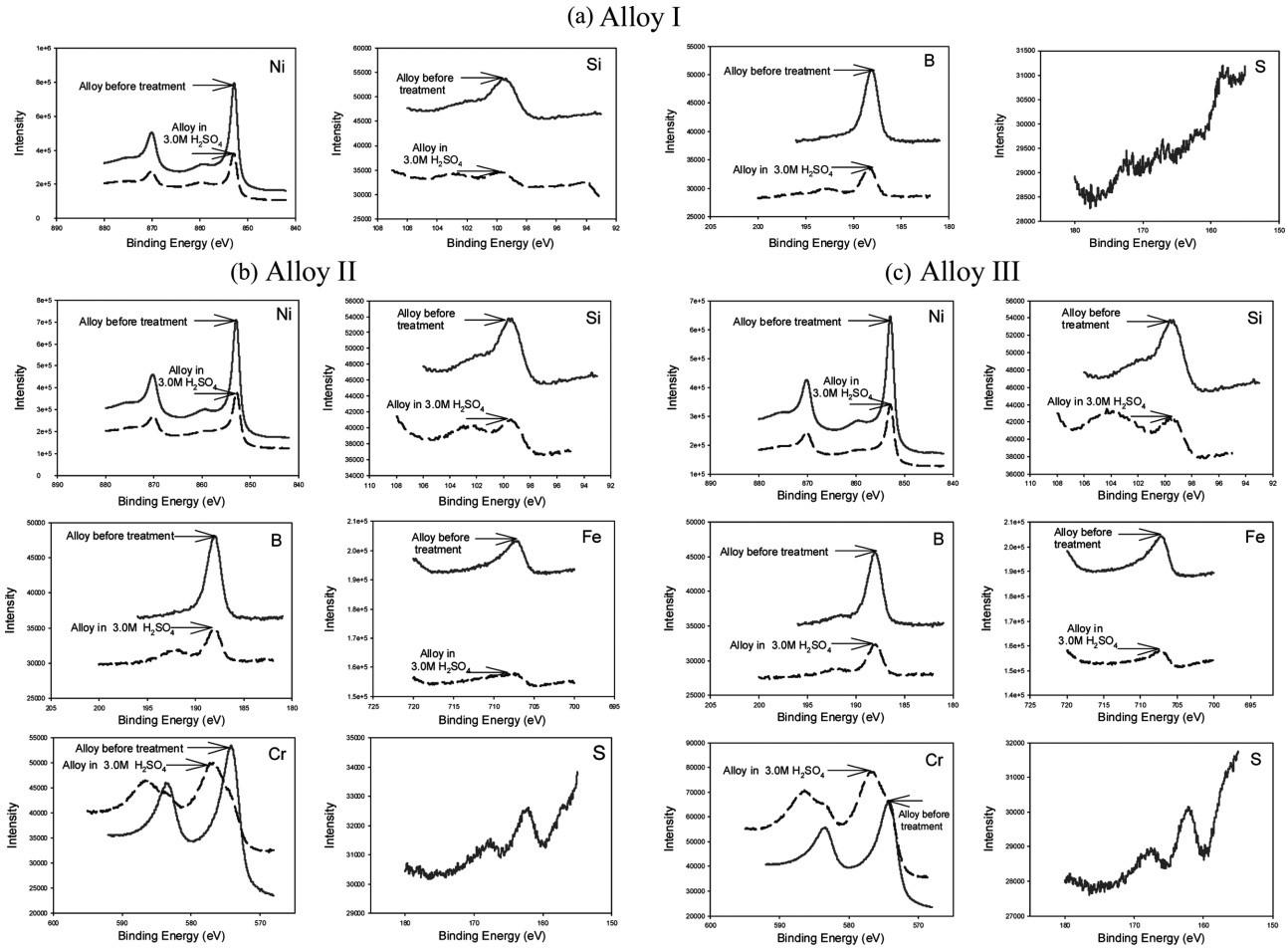

***Fig.* 4.** The photoelectron spectra obtained for the metallic glassy alloys before and after the experiment in 3.0 M H_2SO_4 solution.

***Table* 3.** Electrochemical parameters of polarization for metallic glassy alloys in naturally aerated H_2SO_4 solutions at 30 °C

Alloy	C *(M)*	$-E_{corr}$ *mV/SCE*	$I_{corr} \times 10^2$ *mA/cm²*	E_{cp} *mV/SCE*	E_{pass} *mV/SCE*	E_b *mV/SCE*	$E_{corr} - E_{pass}$ *mV*	I_{cc} *mA/cm²*	I_{pass} *mA/cm²*
I	01.0	213	1.81	143	193	213	406	46.48	34.22
	03.0	236	2.26	253	386	441	622	291.41	140.88
	06.0	178	2.99	272	442	469	620	284.55	181.44
	09.0	239	6.18	269	269	-	508	486.06	485.79
	12.0	222	7.45	304	304	-	536	488.21	483.50
II	01.0	244	0.42	-80	162	865	406	0.910	0.07
	03.0	255	0.58	-18	320	903	575	1.650	0.16
	06.0	213	1.05	74	271	946	484	5.000	0.31
	09.0	215	0.37	179	423	1004	638	16.58	0.12
	12.0	208	0.27	148	413	993	621	11.87	0.10
III	01.0	286	0.073	-159	25	877	311	0.27	0.0075
	03.0	279	0.085	-94	196	898	475	0.39	0.0083
	06.0	196	0.099	-12	290	1079	486	1.88	0.0099
	09.0	204	0.159	39	295	991	499	3.35	0.010
	12.0	210	0.240	62	418	1077	628	10.83	0.019

film (*Scheme* 1) formation on the alloy surface.

Le Canut et al.[29] pointed out that with high [SO_4^{2-}], or in presence of sulphide S^{2-} ions on the layers lead to thinner and porous layer. In our case the pores in protective layer

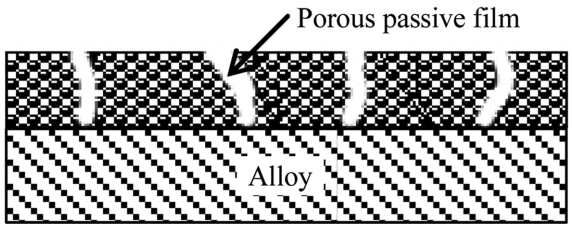

***Scheme* 1.**

possibly due to the presence of nickel sulphides at the interface, which would tend to destabilize the passive layer. These S^{2-} would be the result of sulphate reduction in reducing conditions. The metal surface turned grayish black and the lest solution become green after the polarization experiments.

The current versus potential curves for alloy II (which contains Cr) in H_2SO_4 solutions in the potential range from hydrogen evolution to transpassive dissolution are shown in *Fig*. 3(b). The cathodic polarization curves are shifted towards higher current densities as H_2SO_4 concentration increases. In the anodic part of the potentiodynamic Tafel region followed by a wide constant and low current plateau, which corresponds to a passive region, meaning that the alloy is spontaneously passivated. An active - passive behavior at potential values < -80 mV (SCE) and transpassive phenomena at potential values < 800 mV (SCE) was observed.

The current - potential curves of many metal - electrolyte systems consist of a peak followed by a plateau.[27,31] There is a good agreement that in the rising portion of the curve the metal is dissolved and becomes progressively covered by a blocking species (generally an oxide); current attains a maximum and then drops to a much lower values, once a complete monolayer of the blocking species is formed. Further potential increase, beyond the peak, induces thickening of the oxide film and decrease I_{corr} and I_{pass} values. Corrosion rate on the electrode depends on the diffusion rate and competitive between formation and destroy of protective layer on the electrode.

The kinetic parameters calculated from the polarization curve are summaries in *Table* 3. It is clear from this *Table* that the corrosion rate (I_{corr} values) increase as [H_2SO_4] increase up to 6.0 M, and then the resistance occur.

The onset potential of transpassivity for alloy II in the studied conditions defined as the applied potential slightly increased, the current density started to increase rapidly, this has been found to lie between 800-1000 mV (SCE). The transpassive region is usually associated with the evolution of a gas, particularly oxygen, or metal dissolution and/or breakdown of the passive film leading to localized corrosion. The type of reaction actually operative in a particular case is determined by the nature of metal / electrolyte interface and the potential at which the process ensues.[32] In this study in H_2SO_4 solutions in the transpassive region evolution of gas on the surface was observed on the outside of the formed film which suggested to be oxygen according to the following reaction:[33]

$$4OH^- = O_2 + 2H_2O + 4\bar{e} \quad (1)$$

On the other hand, according to Pourbaix diagram for Cr at potential higher than 1300 mV (SCE), the Cr^{3+} can be oxidized to Cr^{6+} (H_2CrO_4, CrO_4^{2-}, Cr^{6+}- $4H_2O$) to form soluble compounds.[34] The parallel polarization curves at the different acid concentrations in transpassive region indicated that the dissolution posses occur with the same mechanism.

Although there was a systematic increase in E_{cp} values and decrease in the passivation tendency (pronounced increase in I_{cc} values) and potential needed to reach the passive region for alloy II is directly proportional to the acid concentration, values of degree of passive state (I_{pass} values) in the presence of SO_4^{2-} ions indicated deterioration effect of these ions on the passive state at lower concentrations. Adsorption and subsequent in corporation of SO_4^{2-} ions within the passivation oxide layer may lead to the formation of a highly porous protected film allowing high rate of anodic dissolution in the passive region. Diggle et al.[35] and Abdel- Aal and Osman.[36] reported that SO_4^{2-} ions and some other anions allow some anodic dissolution , resulting in the formation of porous layer of significant thickness. This passive layer strongly inhibit the anodic dissolution of the metal on both active and passive region at high concentrations of SO_4^{2-} and makes it's passivation more feasible. At the highest examined concentrations of SO_4^{2-} ion (9.0 and 12.0) M the passivation degree has remarkable increase (decrease in I_{pass} values) suggesting homogeneous adhered non porous protective passive layer on the alloy in spite of low tendency of passivity. This phenomenon assumed that the alloy surface in these solutions covered of both accelerator (S^{-2}) and decelerator (Cr^{3+}) species. The accelerator species decrease the tendency of passivation and decelerator species may increase the passivation degree at high potentials. This behavior shows good agreement between impedance and polarization measurements.

In SO_4^{2-} solutions the test solutions turned colorless to light green yellowish after the polarization experiments, and the alloy surface become gray. The second passive

region observed after transpassive zone at 9.0 and 12.0 M H_2SO_4 can be attributed to the formation of a new oxide phase. Chaudhry and Sing[37] pointed out that the second passive region of Ni is due to either different type of adsorption processes on the electrode surface or oxide film transformation. Such mechanism of transformation is consistent with the assumption that Ni goes in to the solution as Ni^{2+} although the passive film in the transpassive region is considered to be higher valent oxides associated with oxygen evolution.

The cathodic polarization curves of alloy III, *Fig*. 4(c), are shifted regular towards high current densities as *p*H of acid solution decrease. In the anodic region, SO_4^{2-} ion doesn't preventing passive layer formation. The alloy spontaneously passivated after a potential larger than $25 < E_{pass} < 290$ mV (SCE). Passivation current density around $0.0075 < I_{pass} < 0.0099$ $mAcm^{-2}$ as shown in *Table* 3. The active - passive behavior exhibited by the alloy may indicate the role played by competitive adsorption of inhibiting SO_4^{2-} and the aggressive S^{2-} ions. The fixed values of I_{pass} in a wide passive region, about 739 mV(SCE) reflex stability of the passive oxide film.

As shown in *Table* 3, the passivation tendency (I_{cc}) and the degree of passivation (I_P) of alloy III in H_2SO_4 solutions increase with the increase of acid concentration. This may indicated that the increase of acid concentration results in an acceleration of Ni dissolution in both the active and passive regions. Decreasing in the potential needed to reach the passivity region and increasing of I_{pass} value within the passive potential range as the potential shifted in the positive direction can be attributed to the dissolution action of the acid on the passivation oxide layer and / or the increase in the porosity of the oxide layer with the increase in the acid concentration.

The current starts to increase due to transpassive oxidation at $877 < E_b < 1080$ mV(SCE) associated with the evolution of oxygen. No change in the slope of the valtammogram can be seen, this may be indication for the same mechanism of the passive film dissolution. Bojinov et al.[38,39] reported that alloying of Ni with Cr can lead to an increase susceptibility to general corrosion in highly oxidation environments via dissolution of Cr in transpassive region. They also confirm that the transpassive dissolution is a complicated process including electron and ion transport through a surface film. Multi steps electrochemical reactions at the film / solution interface and transport of reaction products in the bulk solution. In addition, they found that the tendency for a secondary passivation in the transpassive region decreases with increasing chromium content in Ni-Cr alloys. This may be connected with the formation of a Cr oxide – based film, on which does not occur on the secondary passivation at high potentials in the transpassive region. Bojinov et al.[39] pointed out that susceptibility of alloy $Ni_{80}Cr_{20}$ for secondary passivation was lower than that for alloy $Ni_{90}Cr_{10}$ in H_3PO_4 solution. This result explains the continuo increasing the dissolution process of alloy III by increase the acid concentration and disappear of secondary passivation comparing to alloy II in the same conditions. As it was explained, before the oxidation of Cr^{3+} to soluble ion (Cr^{3+} - $4H_2O$) at more positive potential reveled the transspassive region at the end of anodic scan. Because of the dissolution of both of Ni and Cr the test solution turned colorless to yellowish at the end of polarization experiment and the alloy surface was smooth but not shiny.

X-ray Photoelectron Spectroscopy (XPS)

XPS analysis was conducted for the specimens before and after impedance and polarizations measurements in 3.0 M HCl open to air experiment at 30C to clarify the difference in surface composition between alloy I (Cr – free), alloy II (7% Cr) and alloy III (13% Cr). The peak binding energy of Ni $2p_{3/2}$ and S $2p_{3/2}$ were approximately 852.8 eV and 162.2 eV, respectively, after the treatment (after the experiment) for alloy I as shown in *Fig*. 4. No change exhibited for Si $2p_{3/2}$ and B $2p_{3/2}$ before treatment (asreceived) and after treatment.

These data confirmed that pseudo passivation was exhibited by the alloy I at 1.0, 3.0 and 6.0 M of H_2SO_4 may attributed to porous nickel sulphide (NiS).

For alloys II and III the peak binding energy of the Ni $2p_{3/2}$ were about 852.9 and 853 eV respectively, before and after the treatment. The Cr 2p spectrum of these two alloys give binding energy of the Cr^m $2p_{3/2}$ and Cr^{ox} $2p_{3/2}$ electrons at 574.2, 575.3 and 576.8, 577 eV respectively which is in agreement with values obtained by many authors[1,2,40-44] Therefore the Cr^{ox} in the surface film will be in the trivalent state. On the other hand, the peak binding energy of $S2p_{3/2}$ electron was observed at 162.9 and 162.5 eV respectively for the alloys II and III indicated the presence of NiS on the alloys surfaces.

According to analysis, the corrosion resistance and the limiting current show in anodic polarization curves of nickel base glassy alloys II and III, is attributable mainly to the formation of hydrated chromium oxyhydroxide film $[CrO_x(OH)_{3-2x}\ nH_2O]$ which formed in range (576.3–579.7 eV).[1,2,9,12,40-45] This oxide layer is associate with little amount of NiS.

Oxide Film Thickness

The average thickness of hydrated chromium oxyhydroxide film on alloy II and III was calculated using equation (2).

$$d_{ox} = \frac{A\varepsilon_o\varepsilon}{C_{ox}} \quad (2)$$

where d_{ox} is the passive layer thickness, C_{ox} is the capacitance of oxide layer, A is the sample surface area (~2.4 cm^2), ε is the dielectric constant of the oxide (assumed to be $\varepsilon = 30$[45-47]), ε_o is the permittivity of free space ($\varepsilon_o = 8.854 \times 10^{-12}$ Fm^{-1}) and C_{ox} is the passive film capacitance is known (in this study n values are nearly to unit so we can assumed that CPE (Q) is equal to C).

The film capacitance values in *Table* 2 the average oxide thickness formed on alloy II and III calculated at different concentration of H_2SO_4 and listed in *Table* 4.

***Table* 4.** Calculation the oxide thickness on alloy II and III from impedance data

C (M)	Thickness of oxide (nm)	
	Alloy II	Alloy III
1.00	3.68	4.93
3.00	3.38	4.77
6.00	3.08	4.27
9.00	4.61	3.80
12.0	4.91	3.76

It is clearer from *Table* 4, that the thickness of the oxide film is several nanometers (nm) and grows linearly with decrease the acids concentration. Also the table explains

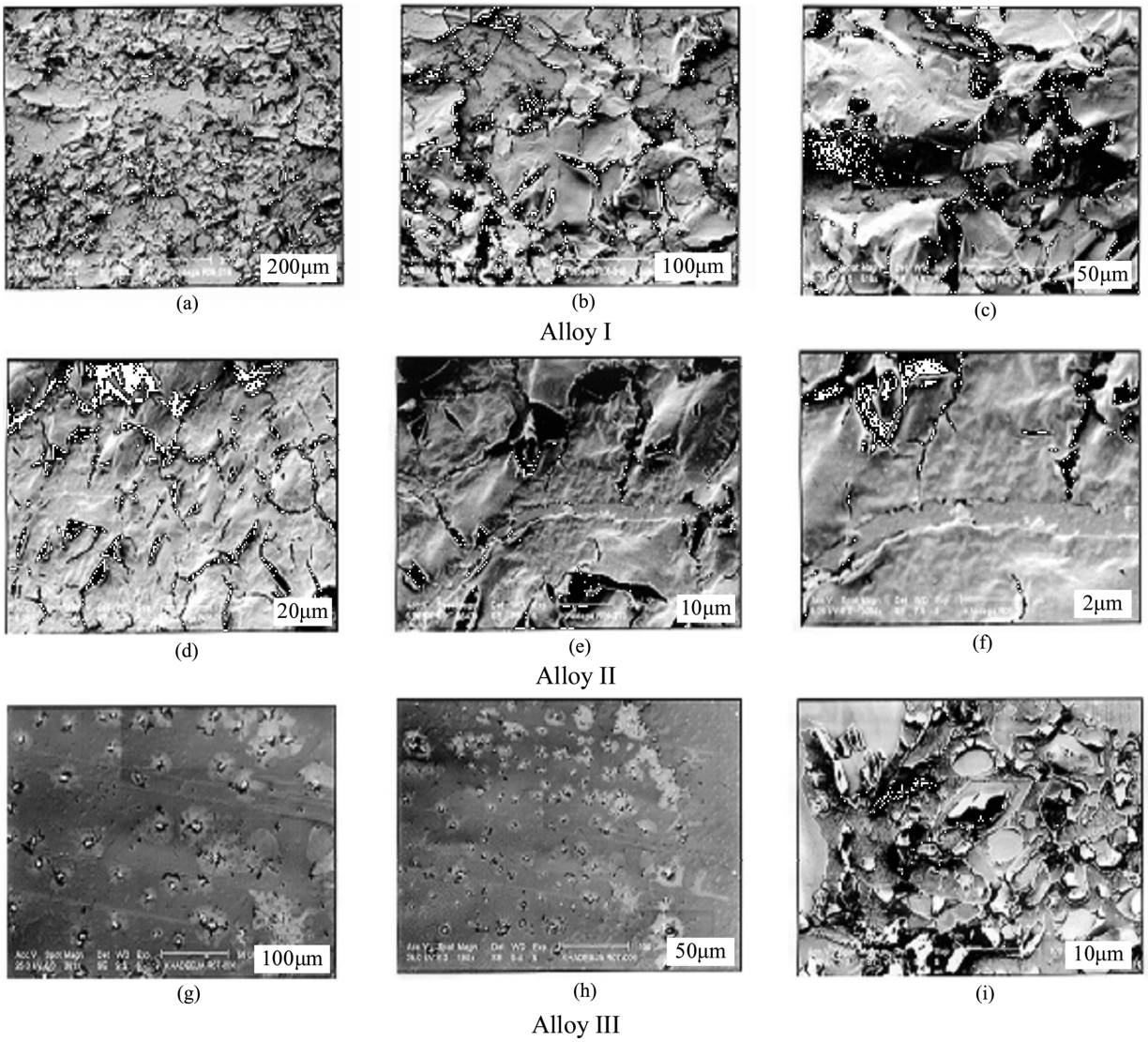

***Fig*. 5.** SEM morphology of for Ni-base metallic glasses alloys at different magnifications in 3.0 M H_2SO_4.

the protective nature of Cr_2O_3[00] which $[CrO_x(OH)_{3-2x}$ $nH_2O]$. The oxide film grows on alloy III is more thicker than that film formed the surface in alloy II. Therefore, the overall decrease in the corrosion resistance and the increase in the capacitance for alloy II were both correlated with the decrease in the effective thickness of the oxide layer.

Scanning Electron Microscope (SEM)

After polarization measurement, the surface of the amorphous alloy I in 3.0 M H_2SO_4 in *Fig*. 5(a) shown a mud-cracked and prose structure of the oxide film . This explained the high passive current density in passive region. The higher magnification is shown the pits and cracks in the oxide layers, *Fig*. 5(b,c), interpreting the presence of pseudo – passivation behavior.

The morphology of Alloy II is observed in *Fig*. 5(d) show the damaged oxide layer after the excrement. The less homogeneous oxide film in *Figs*. 5(e,f) reflect the lower values of n in impedance measurements which confirm the competitive between the accelerator and inhibition process.

Figs. 5(g,h) show the Alloy III surface with nearly compact passive layer covering most of it. The higher magnification, *Fig*. 5(i), is shown some damage in oxide layer. These porous may the center where the O_2 evolutes in transpassive region.

CONCLUSION

The electrochemical behavior of amorphous Ni(Cr)FeSiB alloys in H_2SO_4 solutions at five concentrations from 1.0 to 12.0 M at 30 ^oC were investigated. The following conclusions can be withdrawn:

1. Increase of H_2SO_4 concentration increases the corrosion rate of alloy I and III. Critical concentration behavior appeared in alloy II.

2. Pseudo - passive film formed on the alloy I (Cr free alloy) in low concentrations of H_2SO_4 solutions may attributed to grayish black color porous nickel sulphide (NiS).

3. Chromium-bearing alloys show active - passive region and spontaneously passivated with low passive current densities at all studied acid solutions, and the passive region become wider and more stable in low concentrations.

4. The formation of a hydrated chromium oxyhydroxide passive film on the amorphous alloys II and III surface is responsible for their high corrosion resistance.

5. In spite of beneficial effect of Cr for corrosion resistance, it can lead to increase susceptibility to general corrosion in highly oxidizing environment. In contract, the tendency of secondary passivation at high potentials in the transpassive region decreases with increasing Cr content due to the dissolution of chromium compounds at potentials higher than 1300 mV(SCE).

6. The low CPE (Q) values in the case of alloy III reflex the high capacitive behavior of the alloy surface and thicker oxide layer on this alloy compared with alloy II.

Acknowledgments. The authors wish to express their gratitude to Dr. Hartmann Thomas from Vacuumschmelze company for supplying the nickel base alloys of this research and to Kink Abdulaziz City of Science and Technology (KACST) for supporting this study under postgraduate project (GSP-14-105).

REFERENCES

1. Naka, M.; Hashimoto, K.; Masumoto, T. *J. Non-Cryst. Solids* **1979**, *34*, 257.
2. Hashimoto, K. Passivity of Metals and Semiconductors, Proc. 5th Int. Symp. Passivity. Froment M., Ed.; Elsevier: Amsterdam, **1983**, p 247.
3. Scully, C. Passivity of Metals and semiconductors, Proc. 5th Int. Symp. Passivity. Froment M., Ed.; Elsevier: Amsterdam, **1983**, p 253.
4. Lee, H. J.; Akiyama, E.; Habazaki, H.; Kawashima, A.; Asami, K.; Hashimoto, K. *Corros. Sci.* **1995**, *37*, 1313.
5. Lee, H. J.; Akiyama, E.; Habazaki, H.; Kawashima, A.; Asami, K.; Hashimoto, K. *Corros. Sci.* **1997**, *39*, 321.
6. Habazaki, H.; Sato, T.; Kawashima, A.; Asami, K.; Hashimoto, K. *Mater. Sci. Eng.* **2001**, *304-306*, 696.
7. Pardo, A.; Otero, E.; Merino, M. C.; Lopez, M. D.; Vazquez, M.; Agudo, P. *Corros. Sci.* **2002**, *44*, 1193.
8. Zhang, T.; Pang, S.; Asami, K.; Inoue, A. *Mater. Trans*. **2003**, *44*, 2322.
9. Hashimoto, K.; Asami, K.; Kawashima, A.; Habazaki, H.; Akiyama, E. *Corros. Sci.* **2007**, *49*, 42.
10. Matsuura, M.; Fujita, T.; Kawashima, A.; Yuqiao, Z.; Kimura, H.; Guan, P.; Chen, M.; Inoue, A., Konno, K.; Asada, K.; *J. Alloys Compd.* **2010**, *496*, 135.
11. Rife, G.; Chan, P. C. C.; Aust, K.T.; Waseda, Y. *Mater. Sci. Eng*. **1981**, *48*, 73.
12. Mitsuhashi, A.; Asami, K.; Kawashima, A.; Hashimoto, K. *Corros. Sci.* **1987**, *27*, 957.
13. Lian, K.; Thorpe, S. J.; Kirk, D. W. *Electrochim. Acta* **1992**, *37*, 169.
14. Gassa, L. M.; Vilche, J. R.; Barbosa, M. R. *Mater. Sci. Forum* **1995**, *192*, 825.
15. Lee, H. J.; Akiyama, E.; Habazaki, H.; Kawashima, A.; Asami, K.; Hashimoto, K. *Corros. Sci.* **1996**, *38*, 469.
16. Pang, S.; Shek, C. H.; Zhang, T.; Asami, K.; Ineue, A. *Corros. Sci.* **2006**, *48*, 625.
17. Katagiri, H.; Meguro, S.; Yamasaki, M.; Habazaki, H.;

Sato, T.; Kawashima, A.; Asami, K.; Hashimoto, K. *Corros. Sci.* **2001**, *43*, 183.
18. Pang, S.; Zhang, T.; Asami, K.; Inoue, A. *Mater. Trans.* **2002**, *43*, 1771.
19. Pang, S.; Zhang, T.; Asami, K.; Inoue, A. *Mater. Sci. Eng.* **2004**, *375*, 368.
20. Pang, S.; Shek, C. H.; Asami, K.; Inoue, A.; Zhang, T. *J. Alloys Compd.* **2007**, *434-435*, 240.
21. Arab, S. T. *Orient. J. Chem.* **2007**, *23*, 777.
22. Arab, S. T.; Emran, K. M.; Al-Turaif, H. A. *J. Saudi Chem. Soc.*, in Press. accepted Manuscript, available online 12 June 2011. http://www.sciencedirect.com/science/article/pii/S1319610311001190
23. Boukamp, B. A. *Equivalent Circuits (User Manual)*; University of Twente: The Netherlands, 1989.
24. Hukovic, M. M.; Omanvic, S. *J. Electroanal. Chem.* **1998**, *455*, 181.
25. Girault, P.; Grosseau-Poussard, J. L.; Dinhut, J. F.; Marechal, L. *Nucl. Instrum. Methods Phys. Res., Sect. B* **2001**, *174*, 439.
26. Martini, E. M. A.; Amaral, S. T.; Muller, I. L. *Corros. Sci.* **2004**, *46*, 2097.
27. Perez, F. J.; Martinez, L.; Hierro, M. P.; Gomez, C.; Portela, A. L.; Pucci, G. N.; Duday, D. J. Lecomte - Beckers; J. Greday, Y. *Corros. Sci.* **2006**, *48*, 472.
28. Arab, S. T.; Emran, K. M. Influence of Cr addition on the electrochemical behavior of Ni-base metallic glasses in HCl. accepted in *Physical and Chemical News*.
29. Le Canut, J. M.; Maximovitch, S.; Dalard, F. *J. Nucl. Mater.* **2004**, *334*, 13.
30. Goncalves, R. S.; Azambuja, D. S.; Lucho, A. M. S. *Corros. Sci.* **2002**, *44*, 467.
31. Fontana, M. G. *Corrosion Engineering*, 3th ed.; Mc Graw-Hill; New York, 1987.
32. Singh, V. B.; Gupta, A. *Mater. Chem. Phys.* **2004**, *85*, 12.
33. West, J. M. *Electrodeposition and Corrosion Processes*; Van Nostrand Reinhold Company: New York, 1970.
34. Pourbaix, M. *Atlas of Electrochemical Equilibria in Aqueous Solutions*; Pergamon Press Inc.; New York, 1966.
35. Diggle, J. W.; Downic, T. C.; Gouding, C. W. *Chem. Rev.* **1969**, *65*, 365.
36. Abd El Aal, M. S.; Osman, A. H. *Corrosion* **1980**, *36*, 591.
37. Chaudhary, R. S.; Singh, A. *Br. Corros. J.* **1993**, *28*, 277.
38. Bojinov, M.; Fabricius, G.; Kinnunen, P.; Laitinen, T.; Makela, K.; Saario, T.; Sundholm, G. *Electrochim. Acta* **2000**, *45*, 2791.
39. Bojinov, M.; Tzvetkoff, T. *J. Phys. Chem.* **2003**, *107*, 5101.
40. Hashimoto, K. Passivity of Metals and Semiconductors, Proc. 5th Int. Symp. Passivity. M. Froment, Ed.; Elsevier: Amsterdam, 1983, p 235.
41. Moffat, T. P.; Latanision, R. M. *J. Electrchem. Soc.* **1992**, *139*, 1869.
42. Macdonald, D. D.; Sun, A.; Priyantha, N.; Jayaweera, P. *J. Electroanal. Chem.* **2004**, *572*, 421.
43. Gray, J. J.; El Dasher, B. S.; Orme, C. A. *Surf. Sci.* **2006**, *600*, 2488.
44. Ogihara, H.; Udagawa, K.; Saji, T. *Surf. Coat. Technol.* **2012**, *206*, 2933.
45. Zhang, B. P.; Habazaki, H.; Kawashima, A.; Asami, K.; Hashimoto, K. *Corros. Sci.* **1992**, *33*(10), 1519.
46. Zhang, B. P.; Habazaki, H.; Kawashima, A.; Asami, K.; Hashimoto, K. *Corros. Sci.* **1992**, *33*(5), 667.
47. Tjong, S. C.; Chu, P. K. *Surf. Coat. Technol.* **2007**, *201*, 6781.